Silicon-based composite anodes for Li-ion rechargeable batteries†

Wei Wang,[a] Moni Kanchan Datta[a] and Prashant N. Kumta*[ab]

Received 10th April 2007, Accepted 14th June 2007
First published as an Advance Article on the web 25th June 2007
DOI: 10.1039/b705311h

Si–C and Si–C–Al composite powders have been synthesized by thermal treatment of high-energy mechanically-milled composite precursors comprising graphite, silicon, aluminium and several types of polymers such as poly(acrylonitrile), poly[(*o*-cresylglycidyl ether)-*co*-formaldehyde] resin and poly(methacrylonitrile). The polymers have been used to suppress the interfacial diffusion reactions between graphite, silicon and aluminium, which otherwise lead to the formation of electrochemically-inactive SiC and Al_4C_3 intermetallics during high-energy mechanical milling. The resultant Si–C composite obtained after thermal treatment of mechanically milled powders of nominal composition [52.5 wt% C]–[17.5 wt% Si]–[8 wt% PAN]–[22 wt% resin] exhibits a reversible capacity of $\sim$630 mA h g^{-1} with excellent capacity retention when cycled at a rate of $\sim$160 mA g^{-1}. On the other hand, the Si–C–Al composite of nominal composition [52.5 wt% C]–[14 wt% Si]–[3.5 wt% Al]–[30 wt% PMAN] exhibits a reversible capacity of $\sim$650 mA h g^{-1} up to 30 cycles at a charge/discharge rate of $\sim$340 mA g^{-1}. Scanning electron microscopy analysis of electrochemically-cycled electrodes indicates that the microstructural stability and the structural integrity of the Si–C and Si–C–Al composite is retained during electrochemical cycling, contributing to the good cyclability demonstrated by the composites.

1. Introduction

Li-Ion batteries have been the most widely used portable power sources for consumer electronic devices since 1991 because of their high energy-density and flexible design. While graphite, which exhibits a theoretical capacity of $\sim$372 mA h g^{-1}, is the preferred anode (negative electrode) used in commercial Li-ion batteries, considerable research has been conducted recently to identify different materials as possible alternative anodes exhibiting higher capacity and lower irreversibility.[1–3] Since Fuji identified tin oxide nano-composites as potential anode materials in 1996,[4] tin and silicon have been found to be good candidates to replace graphite as negative electrodes for Li-ion batteries, primarily because Sn and Si demonstrate a higher discharge capacity of about $\sim$990 and $\sim$4200 mA h g^{-1}, respectively.[1–3]

Silicon is one of the most attractive and widely-investigated candidate anode materials due to its high theoretical specific capacity of $\sim$4200 mA h g^{-1} corresponding to the fully lithiated composition of $Li_{4.4}Si$, which is ten-fold higher than that of graphite.[2–6] However, silicon exhibits several phase transitions during the lithium alloying and de-alloying processes, undergoing severe crystallographic volume changes. The mechanical strain generated in the process leads to cracking and crumbling of the electrode, which results in the failure of the anode within a few cycles due to loss of electronic contact between the electrochemically active particles.[7] In an attempt to improve the cyclability of the silicon-based anode, second phase components have been introduced to form *ex situ* active–inactive composites. The second phase components act as a buffering matrix to accommodate the large volume change of silicon upon cycling.[8–22] Among the different matrix materials studied, graphite has been shown to be a good candidate due to its good electronic conductivity and lubrication characteristics. Si–C composites have attracted considerable interest and the electrochemical performance reported so far appear quite promising.[8–22] In recent years, different particle sizes and crystallographic variants of silicon and carbon have been used as the starting materials to synthesize the Si–C composite. These include nanocrystalline and amorphous silicon, graphite, meso-scale carbon microbeads (MCMB) and disordered carbon.[8–21] Several strategies, such as decomposition of organic precursors,[8–11] high energy mechanical milling (HEMM),[12–17] physical mixing[18,19] and carbon coating on silicon particles[20,21] have also been implemented by a number of groups. Thermal pyrolysis of different silicon-containing polymers, for example, is a widely-studied method for the generation of Si–C composites.[8–12] These composites, however, often suffer from a large irreversible loss ($\sim$50–60%) in the first cycle mainly due to the presence of disordered carbon, and sulfur/oxygen/hydrogen impurities generated during the high temperature decomposition process.

High energy mechanical milling (HEMM) is one of the more commonly adopted approaches for synthesizing Si–C composites.[12–17] Results from the use of different starting carbonaceous materials, such as graphite and disordered carbon, show a high first discharge and charge capacity ($\sim$800–1400 mA h g^{-1}). However, the cycling stability is not as good as the Si–C composite derived from thermal pyrolysis of Si-containing polymers, which may arise due to the large

[a]*Department of Materials Science and Engineering, Carnegie Mellon University, Pittsburgh, Pennsylvania, 15213, USA*
[b]*Department of Biomedical Engineering, Carnegie Mellon University, Pittsburgh, Pennsylvania, 15213, USA*
† This paper is part of a *Journal of Materials Chemistry* theme issue on New Energy Materials. Guest editor: M. Saiful Islam.

particle size of silicon, which substantially fractures because of the extensive volume expansion experienced by silicon during the lithium alloying and de-alloying processes. Our research group has developed a method to generate Si–C based nanocomposites through extended HEMM using polymer additives.[14–17] Composites of silicon, graphite and polymer derived disordered carbon generated by extended HEMM followed by subsequent heat treatment exhibit a high reversible capacity ($\sim$550–750 mA h g^{-1}) and excellent capacity retention.[14–17]

Most recently, another electrochemically-active phase which has a higher theoretical specific capacity than graphite is introduced along with the Si–C system in an attempt to further improve the reversible capacity. Rock and Kumta[22] reported graphite–silicon–tin composite anodes synthesized by HEMM, which demonstrate a reversible discharge capacity as high as $\sim$800 mA h g^{-1} with capacity retention of 1.36% loss per cycle. In addition to Sn and Si, Al, Mg and Sb are also known to react with Li to form electrochemically-active intermetallic phases that can serve as potential Li-ion anodes. Careful analysis of the Al–Li binary diagram[23] shows that Al can react with Li to form three possible alloys, AlLi, Al_2Li_3 and Al_4Li_9. Due to the low atomic weight of Al, the alloy containing the lowest Li content, AlLi, provides a theoretical capacity of $\sim$993 mA h g^{-1} which is identical to the Sn–Li phase ($Li_{22}Sn_5$) containing the largest amount of Li among the Sn–Li alloys. Another advantage of using Al is that it exhibits moderate volume expansion during the alloying/dealloying reaction, which makes it a more attractive alternative to tin. The increase in volume when Al reacts with Li to form AlLi is only 97%, compared to the 676% increase in volume when tin reacts with Li to form $Li_{22}Sn_5$.[24] Despite these favorable characteristics, there has not been much reported on the use of Al as a Li-ion battery anode.

Hamon and co-workers[25] reported on the use of Al as a negative electrode in Li-ion batteries, in which aluminium layers with different thicknesses deposited by thermal evaporation demonstrate a capacity of 1000 mA h g^{-1}. However, only first-cycle information has been reported. Al based compounds, such as AlSb and Fe_2Al_5, prepared through mechanical alloying and arc melting, respectively, have also been studied as potential anode materials for lithium-ion batteries.[26,27] Density functional electronic calculations were also employed by Tillard and co-workers[28] to simulate the phase stability and electrochemical properties of compounds in the Li–Al–Si system, the results of which suggested that Li_9AlSi_3 affords a capacity of about 1040 mA h g^{-1}, exhibiting the best electrochemical performance among the different compounds in the Li–Al–Si ternary alloy system. Recently, Lei *et. al.*[29] reported the effects of particle size on the electrochemical properties of aluminium powders as anode materials. The low expansion of Al during electrochemical charging and discharging of lithium indicates that it could be used as a potential additive to silicon and carbon, providing good electrochemical activity and stability during cycling for use as a lithium-ion anode. This is, however, possible only if the composites can be generated with Al existing as a separate discrete phase without reacting with silicon and carbon to form the inactive carbides and silicides.

In the present study, the potential of Si–C and Si–C–Al based composites as Li-ion battery anode materials is investigated. The Si–C and Si–C–Al based composites have been synthesized by high energy mechanical milling of elemental mixtures of graphite, Si and Al in the presence of different types of polymers such as poly(acrylonitrile) (PAN), poly[(*o*-cresylglycidyl ether)-*co*-formaldehyde] resin and poly(methacrylonitrile) (PMAN) followed by thermal treatment. The resultant composites have been characterized for phase evolution, electrochemical performance, cycling stability and morphology.

2. Experimental

2.1. Materials synthesis

2.1.1. Si–C composite. Mixtures of elemental powders of synthetic graphite (Aldrich, 1–2 micron), Si (Alfa Aesar, −325 mesh), PAN and poly[(*o*-cresylglycidyl ether)-*co*-formaldehyde] based epoxy resin (average $M_n \sim 1{,}080$, Aldrich) of elemental composition [52.5 wt% C]–[17.5 wt% Si]–[8 wt% PAN]–[22 wt% resin] were subjected to mechanical milling in a high energy shaker mill (SPEX CertiPrep 8000 M) up to 15 h in a stainless steel (SS) vial using 20 SS balls of 2 mm diameter ($\sim$20 g) with a ball to powder weight ratio 10 : 1. $\sim$0.16 g of PAN and $\sim$0.44 g of resin was dissolved in $\sim$10 ml *N*-methylpyrrolidinone (NMP) to form a homogeneous polymeric solution. Graphite ($\sim$1.05 g), Si ($\sim$0.35 g), and the polymeric solution were batched in a vial inside an argon filled glove box (Vacuum Atmosphere HE-493, $\sim$10 ppm oxygen and $\sim$0.10 ppm moisture) in order to prevent oxidation of the reactive components during milling. The polymeric solution keeps the ingredients and grinding balls completely submerged. This was helpful to avoid excessive cold welding, agglomeration and temperature build up during milling. In order to decompose the PAN and resin to form PAN and resin based carbon,[16,17] respectively, the mechanically milled powders were thermally treated at 1073 K for 6 h in an ultra high purity argon (UHP-Ar) atmosphere using a heating rate 10 K min^{-1} and a flow rate of 100 mL min^{-1}.

2.1.2. Si–C–Al composite. $\sim$0.5 g PMAN (Scientific Polymer Products) was dissolved in $\sim$10 ml NMP to form a homogenous solution. Commercially-obtained elemental powders of graphite (Aldrich, 1–2 micron), Si (Alfa Aesar, −325 mesh), Al (Aldrich, 99%), and PMAN solution were loaded into a SS vial containing 10 mm diameter SS balls according to a ball to powder weight ratio of 20 : 1 with the PMAN solution covering the reactant mixture and the grinding balls completely inside the vial. The process was also conducted inside the glove box. Composites of Si, C and Al were prepared by HEMM up to 15 h using a SPEX CertiPrep 8000 M high-energy mechanical mill. After drying, the powders were harvested from the mechanical mill and were annealed isothermally at 873 K for 20 h in an UHP-Ar atmosphere using a heating rate 5 K min^{-1} and a flow rate of 100 mL min^{-1}.

2.2. Materials characterization

In order to perform qualitative phase analysis, the milled powders cycled, as well as the heat treated powders, were

characterized by X-ray diffraction (XRD) using the Philips XPERT PRO system with Cu Kα (λ = 0.15406 nm) radiation. The microstructure and morphology of the as prepared electrodes as well as the electrochemically-cycled samples were examined using a scanning electron microscope (SEM). Philips XL-30FEG operating at 20 kV was employed for the SEM observation.

In order to evaluate the electrochemical characteristics, electrodes were fabricated on a copper substrate (Insulectro, electro-deposited, thickness: 175 μm) that was approximately 10 mm in diameter. 82 wt% of the active powder was screened by a 325 mesh screen; 8 wt% acetylene carbon black and 10 wt% of poly(vinylidene fluoride) (PVDF) binder dissolved in NMP were mixed to produce the slurry. The as-prepared slurry then was coated onto the copper foil and dried overnight at 110 °C in a vacuum oven prior to assembling the customized test cell. A 2016 coin cell design was used for the Si–C composite employing lithium foil as counter electrode and 1 M $LiPF_6$ in ethylene carbonate–diethyl carbonate (EC–DEC, 2 : 1 in volume) as the electrolyte. The half cell tested for the Si–C composite were cycled in the voltage range from 0.02 to 1.2 V employing a constant current of ~160 and ~320 mA g^{-1}, and a minute rest period between the charge/discharge cycles using a potentiostat (Arbin electrochemical instrument). On the other hand, a prototype hockey puck cell design was used for testing the Si–C–Al composite employing lithium foil as the counter electrode and 1 M $LiPF_6$ in ethylene carbonate–dimethyl carbonate (EC–DMC, 2 : 1) as the electrolyte. The half cells were cycled from 0.02 to 1.2 V employing a constant current of ~340 mA g^{-1} and a minute rest period between the charge/discharge cycles.

3. Results and discussion

3.1. Si–C composite

Fig. 1 shows the XRD patterns obtained for the [52.5 wt% C]–[17.5 wt% Si]–[8 wt% PAN]–[22 wt% resin] composite precursor after 15 h of milling. The XRD patterns of the 15 h milled sample (Fig. 1) show the presence of graphite and silicon without any detectable amount of SiC. The formation of electrochemically-inactive SiC, which formed during high energy mechanical milling (*e.g.* within ~5 h of mechanical milling in SPEX 8000 shaker mill) of pure graphite and Si, as reported in our earlier paper,[16] is bypassed in the presence of the polymeric solution. Graphite, which transforms to an amorphous structure during high-energy mechanical milling[16] (*e.g.* within ~2 h of milling in SPEX 8000 shaker mill) retains its graphitic structure in the presence of the polymeric solution even after ~15 h of milling. The present results clearly suggest that the polymeric solution, which is expected to be absorbed and coated on the newly formed surfaces of the particles generated by the processes of repeated cold welding and fracture during mechanical milling, acts as a diffusion barrier to the interfacial diffusion reaction between graphite and Si to form electrochemically-inactive SiC and also reduces the amorphization kinetics of graphite.

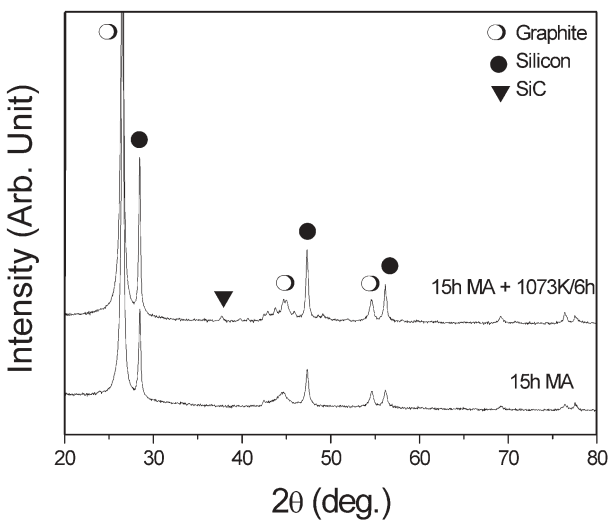

Fig. 1 XRD patterns of [52.5 wt% C]–[17.5 wt% Si]–[8 wt% PAN]–[22 wt% resin] generated after 15 h of milling and after thermal treatment at 1073 K for 6 h in UHP-Ar following the 15 h of milling.

However, the presence of PAN and resin is undesirable in the final product due to their poor electrical conductivity and poor lithium ion diffusivity, which are expected to deteriorate the electrode performance of the Si–C composite. Hence, it is necessary to pyrolyze and convert the polymer to carbon at a suitable temperature to prevent the formation of SiC. The carbon formed should be at most electrically conductive and also exhibit good lithium ion diffusivity.[16,17] Based on our earlier DTA/TGA results of PAN and resin,[16,17] the 15 h milled powder has been thermally treated at 1073 K for 6 h in UHP Ar atmosphere to decompose the polymer to form PAN and resin based carbon. The XRD patterns of the powder thermally treated at 1073 K, shown in Fig. 1, show the characteristic peaks corresponding to graphite and Si with a small amount of SiC. The composition of the Si–C composite after thermal treatment at 1073 K is estimated based on the 37% yield of PAN based carbon[16] and 23% yield of resin based carbon[17] determined from thermal analysis and considering no weight loss of graphite and silicon during thermal treatment. The composition of the composite is determined to be approximately [67.3 wt% C]–[22.4 wt% Si]–[3.8 wt% PC]–[6.5 wt% RC], which corresponds to the atomic percent composition of [77.2 at% C]–[11 at% Si]–[4.4 at% PC]–[7.4 at% RC], where PC and RC denote the PAN-based and resin-based carbon, respectively.

Fig. 2 shows the variation of specific capacity *vs.* cycle number of the Si–C composite cycled at a constant current of 160 and 320 mA g^{-1}. The Si–C composite cycled at 160 mA g^{-1} shows a 1st discharge and 1st charge capacity of ~827 and ~608 mA h g^{-1}, respectively, with an irreversible loss of ~27%. On the other hand, the Si–C composite cycled at 320 mA g^{-1} shows a 1st discharge and 1st charge capacity of ~680 and ~509 mA h g^{-1}, respectively, with an irreversible loss of ~25%. As shown in Fig. 2, the reversible capacity of Si–C composite cycled at 160 and 320 mA g^{-1} increases with subsequent cycles in the initial cycles (up to the 5th cycle). This result clearly suggests that the electrochemically-active materials (Si and C) are not completely utilized in the first few cycles, which may be due to the slow initial electrochemical kinetics of lithium with silicon (which reach an optimal state

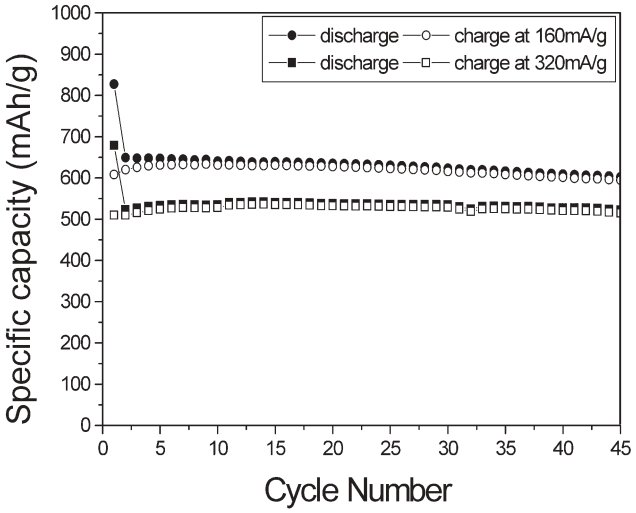

Fig. 2 Plot of specific capacity with cycle number of Si–C derived composite electrode cycled at a rate of ~160 and ~320 mA h g^{-1}.

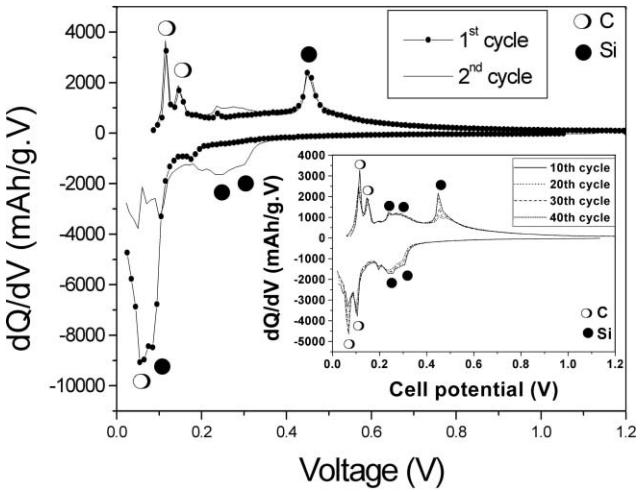

Fig. 3 Differential capacity with cell potential curves of Si–C derived composite electrode after 1st and 2nd cycle, and after 10th, 20th, 30th and 40th cycle (inset figure).

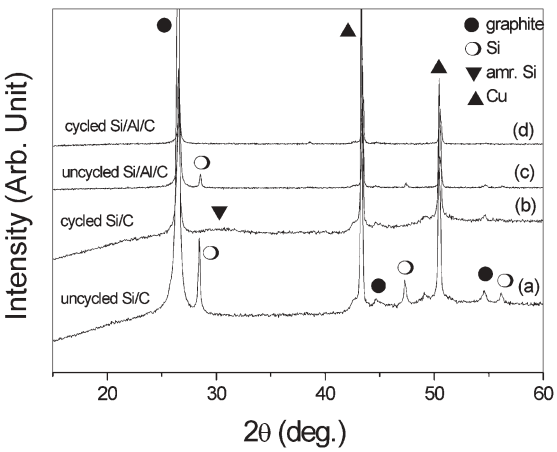

Fig. 4 XRD patterns of Si–C and Si–C–Al composite electrode before (a and c) and after (b and d) electrochemical cycling.

only after several cycles). After the 5th cycle the Si–C composite cycled at 160 mA g^{-1} exhibits an optimal reversible capacity of ~630 mA h g^{-1} with excellent capacity retention of 0.12% loss per cycle up to the 45th cycle (~594 mA h g^{-1} after the 45th cycle). The composite cycled at 320 mA g^{-1} shows an optimal reversible capacity of ~530 mA h g^{-1} after the 5th cycle and exhibits ~0.1% loss per cycle up to the 45th cycle (~515 mA h g^{-1} after the 45th cycle). The above results show that the capacity retained at the discharge/charge rate of 320 mA g^{-1} (~C/1.66) is approximately 84% in comparison to the discharge/charge rate of 160 mA g^{-1} (~C/4 rate). The decrease in the reversible capacity with increasing charge/discharge rate mainly arises due to the slow rate of diffusion of Li ion through the composite. The diffusion rate of Li ion and, as a result, the rate capability is expected to be enhanced by synthesizing a Si–C nanocomposite comprising nanometer sized Si particles dispersed homogeneously in the high-rate-capability synthetic flake graphite (SFG) matrix. The electrochemical performance of the Si–C nanocomposite comprising nanometer sized Si particles and high rate capability SFG graphite will be published very shortly.

The differential capacity plot of Si–C composite cycled at ~160 mA g^{-1} (Fig. 3) shows that both Si and graphite are active. In addition to silicon and graphite, disordered carbon [generated from PAN (PC) and resin (RC)] is also expected to contribute to the overall capacity of the composite. After the 1st cycle, the appearance of peaks corresponding to ~0.09, ~0.24 and ~0.29 V suggests that the crystalline Si transforms to amorphous Si after the 1st cycle, whereas graphite retains its graphitic structure. The formation of amorphous silicon and the preservation of the graphitic structure during electrochemical cycling has been confirmed by XRD analysis of the cycled samples. The XRD patterns (Fig. 4) of the cycled electrode after the 5th cycle shows the peaks corresponding to graphite and a very broad peak corresponding to amorphous silicon along with the copper substrate. These results confirm the presence of amorphous silicon in the differential capacity plots shown in Fig. 3. The formation of amorphous Si during electrochemical cycling of crystalline Si is also confirmed by other workers.[30] After the 1st cycle, the peak intensity corresponding to the reaction of Li ion with amorphous Si (~0.09, ~0.24 and ~0.29 V) remains almost unchanged with cycling (inset in Fig 3), which suggests the excellent retention of capacity of the composite with cycling. The reversible capacities of graphite, PAN based carbon, and resin based carbon determined from individual testing of cells were ~300 , ~300 and ~250 mA h g^{-1}, respectively, cycled at 160 mA g^{-1}. Therefore, the expected contribution on the overall capacity of the composite due to the presence of graphite (77.2 at%), PAN based carbon (4.4 at%) and resin based carbon (7.4 at%) will be approximately ~231, ~13 and ~19 mA h g^{-1}, respectively. On the other hand, the expected contribution to the overall capacity of the composite due to the presence of Si (11.0 at% Si) is approximately ~440 mA h g^{-1}. Therefore, the overall expected capacity of the Si–C composite will be ~700 mA g^{-1} which is very close to the reversible capacity (~630 mA h g^{-1}) of the composite cycled at ~160 mA g^{-1}.

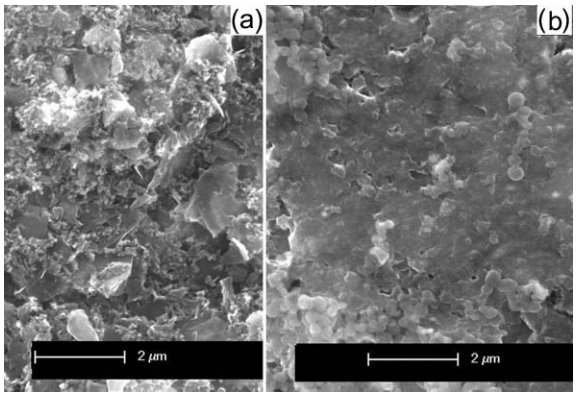

Fig. 5 SEM micrograph of Si–C composite electrode (a) before (b) after cycling for 45 cycles.

The excellent capacity retention observed with the Si–C composite is probably due to the maintenance of the structural integrity of the electrode during the alloying and dealloying processes. The SEM micrograph of the uncycled and cycled samples of Si–C composite cycled at $\sim$160 mA g^{-1} is shown in Fig. 5. The SEM image of Si–C composite after cycling (Fig. 5b) shows that there is no microstructural failure or cracking of the Si–C composite even after 45 cycles although the formation of the solid electrolyte interphase (SEI) on the particles' surface appears to be evident. This can be seen from the appearance of a smooth surface topography on the electrode surface of the cycled samples (Fig. 5b) due to the coverage of the active particles by the SEI layer. The excellent microstructural stability of the Si–C composite and structural integrity of the electrode is expected to arise due to the more homogeneous distribution of Si within the graphite matrix during extended milling. In addition, the solution coating by PAN and resin is expected to enhance the wettability between graphite and Si. As a result, the carbon coating obtained by thermal decomposition of PAN and resin may improve the mechanical properties of the composite by enhancing the interface adhesion/bonding between Si and graphite. The interface characters and the mechanical properties of the Si–C composite are currently in progress and will also be published very shortly. Thus, the PAN and resin based carbon coating is expected to improve the capacity retention due to enhancement of the interface strength between graphite and silicon. Nevertheless, based on the above results, it can be concluded that the Si–C composite prepared from graphite, Si and, PAN and resin based polymeric solution by mechanical milling followed by thermal treatment is promising for use as anodes for Li ion battery applications.

3.2. Si–C–Al composite

Dry milling was first conducted, in which the mixture of elemental graphite, Si and Al powders were subjected to mechanical milling for up to 4 hours. Fig. 6 shows the XRD patterns of the [60 wt% C]–[14 wt% Si]–[26 wt% Al] composite obtained after milling for different periods of time. With increasing milling time, the peak intensity of Si and Al decreases. After 4 hours of milling, almost all the Al has been consumed. However, the formation of nanocrystalline SiC and

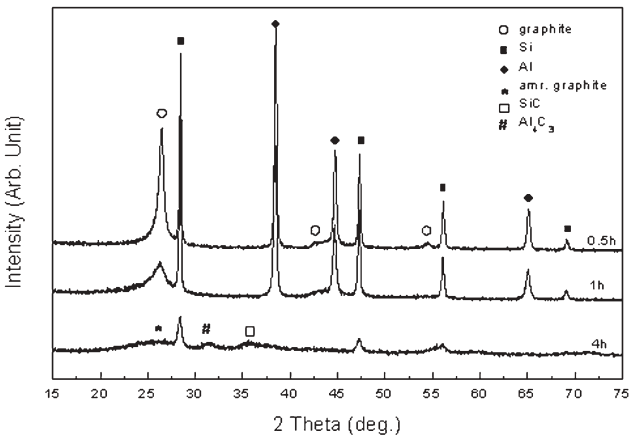

Fig. 6 XRD pattern of [60 wt% C]–[14 wt% Si]–[26 wt% Al] composite generated after milling for different periods of time.

Al_4C_3 of crystallite size $\sim$5 nm, calculated from the most intense peaks of (012) at 31.19 degrees for Al_4C_3 and (102) at 35.7 degrees for SiC, respectively (using the Scherrer equation), can be observed. Within 4 hours of milling, the crystalline structure of graphite also collapses to an amorphous form due to the defect-induced melting of crystalline graphite.[31,32] Therefore, the powder harvested after 4 hours of milling has been identified as a mixture of amorphous graphite and nanocrystalline SiC and Al_4C_3. Similar results have been reported in the case of dry milling of Si and graphite by Datta and Kumta.[16,17]

The variation in specific gravimetric capacity with cycle number for the [60 wt% C]–[14 wt% Si]–[26 wt% Al] composite sample cycled at a rate of $\sim$340 mA g^{-1} of the electrode prepared with powders obtained after different milling times are shown in Fig. 7. As shown in the XRD pattern discussed above, the weight fraction of active Si decreases with increasing milling times, which is manifested as a decrease in the first insertion capacity with increasing milling times as displayed in Fig. 7. The theoretical capacity of [60 wt% C]–[14 wt% Si]–[26 wt% Al] composite sample was calculated to be $\sim$760 mA h g^{-1}. The first charge capacity of the sample milled

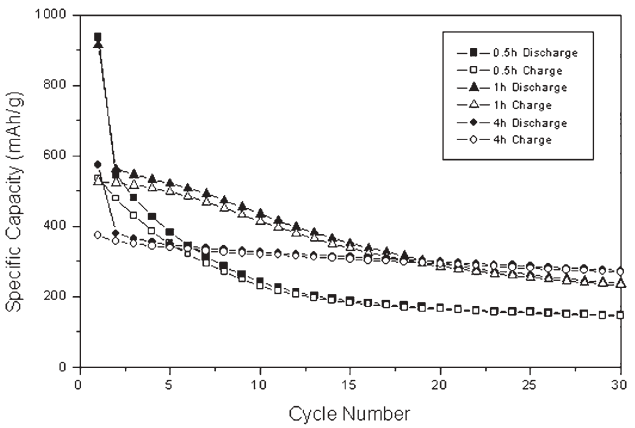

Fig. 7 Plot of specific capacity with cycle number of [60 wt% C]–[14 wt% Si]–[26 wt% Al] composite obtained after different periods of milling, and cycled at a rate of 340 mA g^{-1}.

for 30 min reaches 536 mA h g^{-1} which decreases to 373 mA h g^{-1} for the sample milled for 4 h. The discrepancy between the calculated theoretical capacity and the first charge capacity, and the reduction in first charge capacity as milling time increases (apart from other reasons) is an indication of the formation of the electrochemically inactive SiC and Al_4C_3 phases as revealed by the XRD analysis. The variation of the overall fade in capacity of the Si–C–Al composite with the milling time is also plotted in Fig. 8, which shows that the capacity retention improves significantly as the milling time increases from 30 min to 4 h.

The electrode prepared from the powder milled for 4 h showed the best capacity retention with a fading rate of ~0.8% capacity loss per cycle up to 30 cycles. The improved cycling stability is attributed to the presence of nanocrystalline SiC and Al_4C_3, the electrochemically inactive components generated *in situ* during the HEMM process, which act as a filler providing improvement in the matrix strength and rigidity.[13] In addition, the composite obtained after 30 min of milling exhibits a rapid fade in capacity in the first 10 cycles, which is commonly observed in the cycling performance of the silicon based anode.[12,16] This result also suggests that 30 min of mechanical milling is not adequate to induce mixing between the Si and graphite particles to form a homogeneous composite and, therefore, the Si and graphite particles still remain as distinct phases. This rapid decline of capacity is less pronounced in the sample milled for 1 h and is not observed from the sample obtained after 4 h of milling, which suggests that a more homogeneous distribution of Si, Al and graphite resulting from a longer milling time may be preferred for obtaining a better cycling performance.

As shown in Fig. 8, there is also a reduction in the irreversible loss with extended milling, possibly due to the formation of inactive SiC and Al_4C_3 phases. This trend is also manifested in Fig. 9, in which the first cycle of the differential capacity with cell potential is plotted for the sample milled for 0.5 and 4 h, respectively. The intensity of the solid electrolyte interphase (SEI) peak at ~0.75 V for the sample milled for 4 h is much lower than that of 0.5 h. Fig. 9 also shows that Si, Al

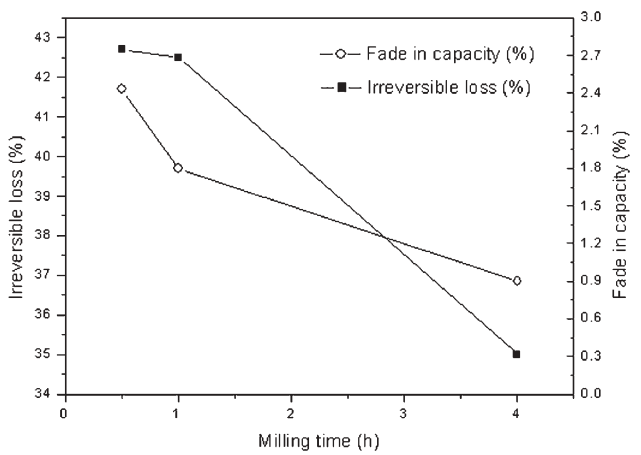

Fig. 8 Variation in fade in capacity and irreversible loss of [60 wt% C]–[14 wt% Si]–[26 wt% Al] composite for different periods of milling time.

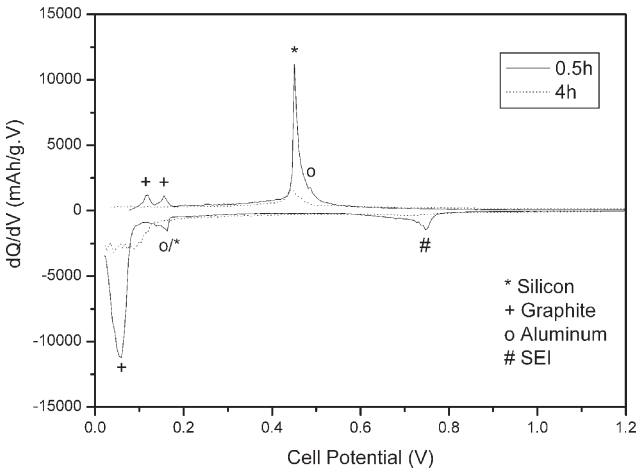

Fig. 9 Plot of the first cycle differential capacity with cell potential of [60 wt% C]–[14 wt% Si]–[26 wt% Al] composite for different periods of milling time.

and graphite are all electrochemically active. Details of the differential capacity with cell potential of Si–C–Al composite will be discussed in the later section below. However, the peak intensities of Si and graphite for the sample milled for 4 h are much weaker than those of the 0.5-h milled sample. Moreover, in the sample milled for 4 h, the peak for Al is not observed. The decreasing intensity of the Si, Al and graphite with increasing milling time once again suggests the formation of SiC and Al_4C_3 phases as discussed above, which consumes the active components and therefore lowers the reversible capacity. From the above discussion, extended milling is clearly warranted to achieve a more homogeneous distribution of the active silicon and aluminium particles in the graphite matrix to improve the capacity retention, thus leading to an enhanced cycle life. However, the mechanochemical reaction between Si, Al, and graphite which results in the formation of SiC and Al_4C_3 and the amorphization of graphite during extended milling must be substantially suppressed in order to achieve a high capacity with a high Si content and low irreversibility with good cyclability.

Different polymers, such as epoxy resin[17] and PAN,[16] have been used as milling additives to act as diffusion barriers between Si and graphite to circumvent the formation of SiC. In this study, extended mechanical milling of Si, Al and graphite has been conducted in the presence of PMAN, serving as a polymer additive performing a similar role as PAN. PMAN has very low yield of carbon residue of ~4% after decomposition at 673 K,[33] which is preferred for improved electrode performance, since most of the carbon generated after high temperature treatment is largely amorphous and non-conducting resulting in large irreversibility, as in the case of PAN.[16] Therefore, the sample was thermally treated at 873 K for 20 h in UHP-Ar to completely decompose PMAN. In order to improve the capacity, the amount of the active component was increased and milling was conducted on a sample of nominal composition [52.5 wt% C]–[14 wt% Si]–[3.5 wt% Al]–[30 wt% PMAN], which corresponds to the actual composition of [75 wt% C]–[20 wt% Si]–[5 wt% Al] after heat treatment considering the 4% yield of PMAN. This corresponds to the

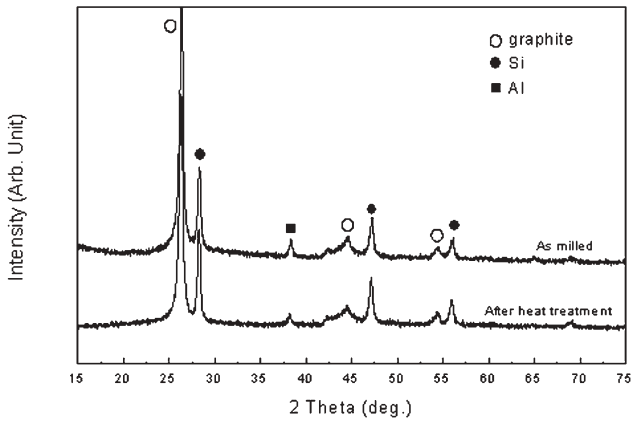

Fig. 10 XRD pattern of [75 wt% C]–[25 wt% Si]–[5 wt% Al] composite generated after milling for 15 hours of milling using PMAN and after thermal treatment at 873 K in UHP-Ar for 20 hours.

atomic percent composition of [87.4 at% C]–[10 at% Si]–[2.6 at% Al].

XRD analysis was conducted on the composite containing [75 wt% C]–[20 wt% Si]–[5 wt% Al] obtained after 15 hours of milling and the XRD pattern is shown in Fig. 10. The as-milled powder consists of crystalline Si, C and Al. It should be noted that SiC and Al_4C_3 phases are not observed in the XRD spectra, which suggests that PMAN is an effective polymer-additive to circumvent the interfacial reaction between Si, Al and graphite particles. The collapse of the crystalline graphite structure to an amorphous form due to the defect-induced breakdown of the graphite lattice[31,32] was also not observed in the XRD spectra, which indicates that the graphite structure is well preserved. The graphite structure is desired over the amorphous state because of the lower irreversibility and better lubrication ability of the graphite to accommodate the volume change of the active phases during cycling. Therefore, the XRD pattern indicates that the Si and Al are well dispersed in the graphite matrix.

The variation in specific gravimetric capacity with the cycle number of the electrode prepared with thermally treated powders is shown in Fig. 11. The Si–C–Al composite cycled at 340 mA g^{-1} shows a 1st charge capacity of 711 mA h g^{-1},

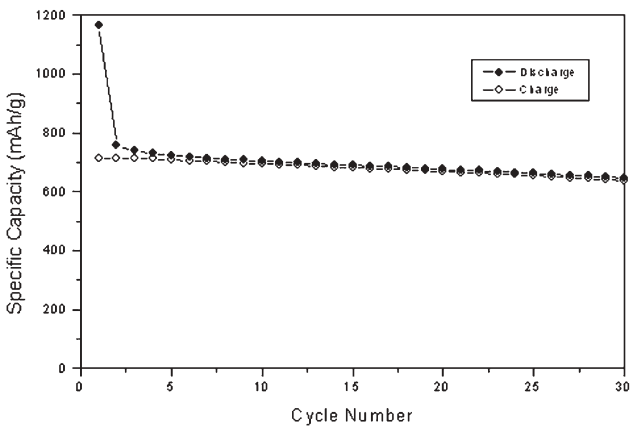

Fig. 11 Plot of specific capacity with cycle number of the Si–C–Al composite electrode cycled at a rate of 340 mA g^{-1}.

which is very close to the expected theoretical capacity of 777 mA h g^{-1} for the composite, calculated assuming a complete reaction of Si with 4.4 Li and Al with 1 Li, with an irreversible loss of ~38%, which is due to the reaction of the electrolyte with the active phases forming the SEI layer, as demonstrated by the peak at ~0.7 V in the differential capacity plot. The Si–C–Al composite exhibits a reversible capacity of ~650 mA h g^{-1} with a capacity loss of 0.3% per cycle up to 30 cycles indicative of very good capacity retention. The differential capacity with cell potential for the composite sample containing [75 wt% C]–[20 wt% Si]–[5 wt% Al] composite obtained after 15 h milling is shown in Fig. 12. Fig. 12 again shows that the Si, Al and graphite phases are all active. Compared with the cyclic voltammogram results published in reference[24] in which Hamon *et al.* reported the electrochemical performance of aluminium thin films *versus* a lithium electrode at 293 K, the aluminium peak at ~0.19 V unfortunately overlaps with one of the silicon peaks. However, the peak at ~0.5 V confirms the electrochemical activity of aluminium. The peaks at ~0.09, ~0.24 and ~0.29 V after the first cycle suggest that the crystalline Si is converted to the amorphous state after the first cycle similar to the Si–C composites discussed earlier. The XRD patterns (Fig. 4) of the Si–C–Al composite electrode after the 5th cycle show the formation of amorphous Si with preserved graphitic structure in the cycled electrode. After the first cycle, the decrease in peak intensity in Fig. 12 (inset), corresponding to the reaction of Li ion with amorphous Si (~0.09, ~0.24, ~0.29 and 0.45 V), indicates the increase in polarization and the resultant fade in capacity due to a reduction in the amount of the electrochemically active components.

Scanning electron microscopy analysis was conducted on the samples before and after electrochemical cycling for 30 cycles in order to investigate any changes in the microstructure or morphology of the particles during the insertion and de-insertion processes. Fig. 13 shows the morphologies of the uncycled and cycled samples of the Si–C–Al electrodes fabricated from the composite containing [75 wt% C]–[20 wt% Si]–[5 wt% Al] obtained after 15 hours milling. The surface of the electrode after 30 cycles is devoid of any visible cracks, which contributes to the structural integrity and the good cycling stability of the electrode after 30 cycles. Moreover, there appears to be no significant change in the morphology of the particles before and after cycling, which indicates no coalescence or aggregation of Si, Al and C particles, therefore exhibiting a good stability of the composite. However, although there is no obvious change in the surface morphology, the existence of a solid electrolyte interphase layer on the surface of the particles cannot be discounted due to the presence of the ~0.7 V peak in the dQ/dV plot as indicated in Fig. 12.

The sample that has been milled for an extended period of time (15 h) in PMAN, followed by thermal treatment, obviously displays significantly improved overall electrochemical performance compared with the dry-milled samples (see Fig. 7). This is largely due to the fact that Si and Al are more homogeneously distributed in the graphite matrix, which may lead to a stronger interfacial contact between silicon, aluminium and carbon, providing a better cycling stability.

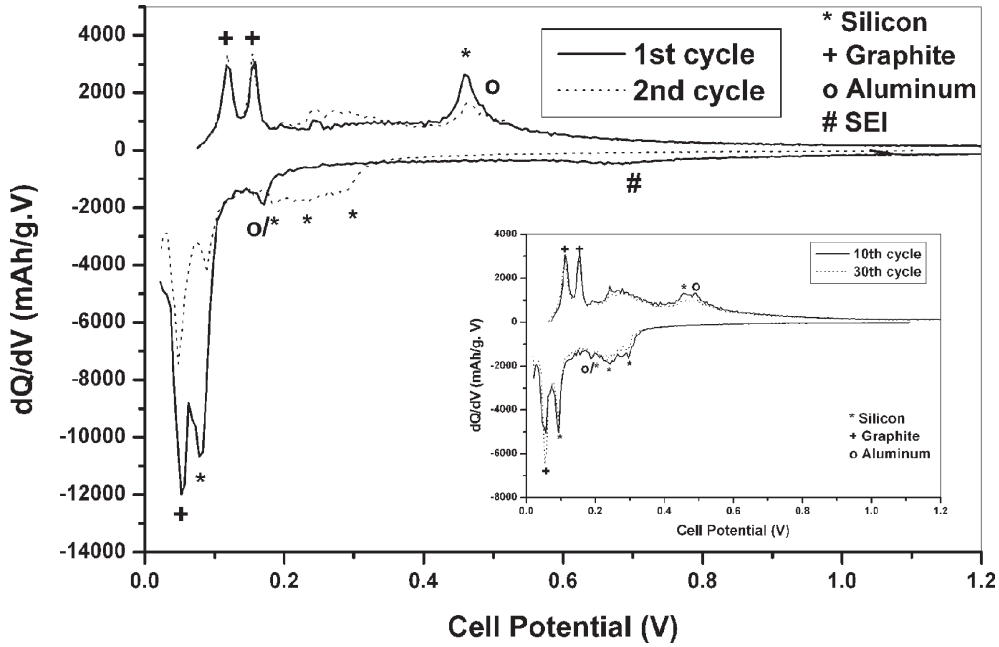

Fig. 12 Plot of differential capacity with cell potential of the Si–C–Al composite electrode after the 1st and 2nd cycle and (inset) after 10th and 30th cycle.

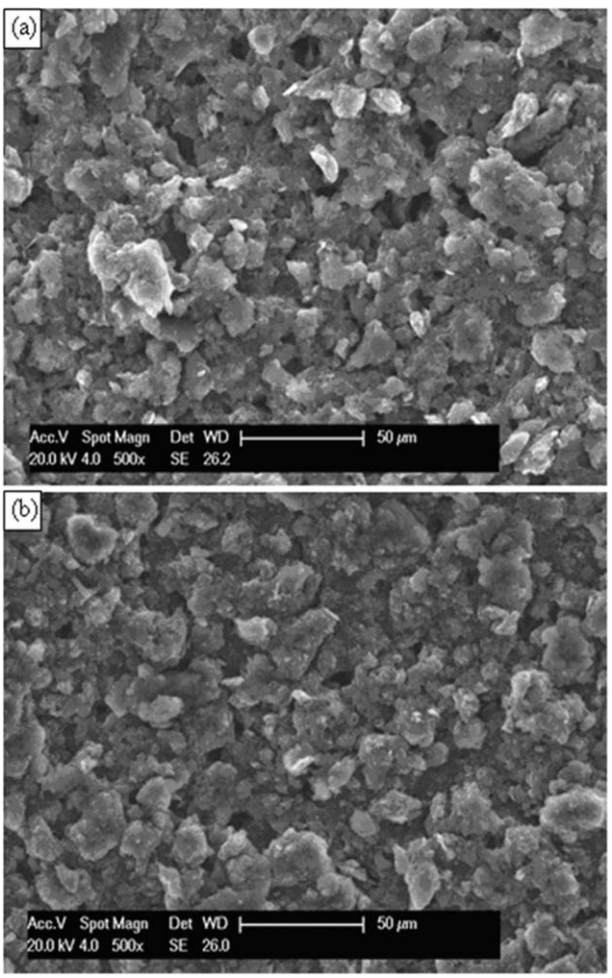

Fig. 13 SEM micrograph of the Si–C–Al electrode (a) before and (b) after cycling for 30 cycles.

This result also suggests that Al appears to be a good active matrix for Li-ion anodes. The fine Al particles that are homogeneously dispersed with the Si in the graphite matrix during the extended milling and thermal treatment may act as a effective buffer to accommodate and cushion the mechanical stresses arising from the expansion and contraction during the alloying and dealloying processes. More detailed studies are, however, warranted to provide further insight into the exact role of Al during mechanical milling, thermal decomposition of the polymer, and subsequent electrochemical cycling of the electrode. It is also possible that the Al–Li phase formed during alloying possesses better mechanical properties and is less brittle compared to the Si–Li phases, thus providing the better capacity retention of the composite electrodes. There is, however, very little confirmation available on the mechanical properties (*e.g.* strength and fracture toughness) of these electrochemically active Li–Al and Li–Si alloys. Hence, more research is clearly needed to understand these critical aspects in these Si–C and Si–C–Al systems.

4. Conclusions

The Si–C and Si–C–Al composite precursors were synthesized by high-energy mechanical milling (HEMM) of elemental Si, Al and graphite in the presence of different kinds of polymeric solution such as PAN, poly[(*o*-cresylglycidyl ether)-*co*-formaldehyde] resin and PMAN. The Si–C composite is synthesized by HEMM of nominal composition [52.5 wt% C]–[17.5 wt% Si]–[8 wt% PAN]–[22 wt% resin] followed by thermal treatment at 1073 K for 6 h in UHP-Ar. The resultant Si–C composite as a lithium ion anode shows a reversible capacity $\sim$630 and $\sim$530 mA h g^{-1} with excellent capacity retention when cycled at a rate of $\sim$160 and $\sim$320 mA g^{-1}, respectively. On the other hand, the dry-milled Si–C–Al composite exhibits improved electrochemical cycling stability with increasing

milling time due to the more homogeneous distribution of Si and Al within the graphite matrix. However, the formation of the electrochemically-inactive nanocystalline SiC and Al_4C_3 consumes the active Si and Al. As a result, the Si–C–Al composite exhibits a decrease in reversible capacity with increase in milling time. HEMM was, therefore, conducted in the presence of PMAN, acting as a diffusion barrier to prevent the interfacial reaction between graphite and Si/Al during the prolonged milling of up to 15 hours followed by a thermal treatment at 873 K for 20 hours in UHP-Ar. The XRD analysis of the Si–C–Al composite indicates the presence of graphite, Si and Al without the formation of SiC and Al_4C_3. A composite of nominal composition [75 wt% C]–[20 wt% Si]–[5 wt% Al], obtained after 15 hours milling, exhibited a reversible capacity of $\sim$650 mA h g^{-1} with a capacity retention of $\sim$0.3% loss per cycle up to 30 cycles. These results suggest that the Si–C and Si–C–Al composites could be promising alternative anodes to carbon.

Acknowledgements

The authors acknowledge the support of Changs Ascending, Taiwan and the Pennsylvania Infrastructure Technology Alliance (PITA).

References

1 M. Winter and J. O. Besenhard, *Electrochim. Acta*, 1999, **45**, 31.
2 B. A. Boukamp, G. C. Lesha and R. A. Huggins, *J. Electrochem. Soc.*, 1981, **128**, 725.
3 J. Maranchi, O. I. Velikokhatnyi, M. K. Datta, I. S. Kim and P. N. Kumta, in *Chemical Processing of Ceramics, 2nd edn*, ed. B. Lee and S. Komarneni, CRC Press, Taylor and Francis, 2005, p. 667.
4 Y. Idota, T. Kubota, A. Matsufuji, Y. Maekawa and T. Miyasaka, *Science*, 1997, **276**, 1395.
5 K. Amezawa, N. Yamamoto, Y. Tomii and Y. Lto, *J. Electrochem. Soc.*, 1998, **145**, 1986.
6 W. J. Weydanz, M. Wohlfahrt-Mehrens and R. A. Huggins, *J. Power Sources*, 1999, **81–82**, 237.
7 J. H. Ryu, J. W. Kim, Y. E. Sung and S. M. Oh, *Electrochem. Solid-State Lett.*, 2004, **7**, A306.
8 A. M. Wilson and J. R. Dahn, *J. Electrochem. Soc.*, 1995, **142**, 326.
9 A. M. Wilson, W. Xing, G. Zank, B. Yates and J. R. Dahn, *Solid State Ionics*, 1997, **100**, 259.
10 J. Yang, B. F. Wang, K. Wang, Y. Liu, J. Y. Xie and Z. S. Wen, *Electrochem. Solid-State Lett.*, 2003, **6**, A154.
11 Z. S. Wen, J. Yang, B. F. Wang, K. Wang and Y. Liu, *Electrochem. Commun.*, 2003, **5**, 165.
12 C. S. Wang, G. T. Wu, X. B. Zhang, Z. F. Qi and W. Z. Li, *J. Electrochem. Soc.*, 1998, **145**, 2751.
13 G. X. Wang, J. Yao and H. K. Liu, *Electrochem. Solid-State Lett.*, 2004, **7**, A250.
14 Il-seok Kim, G. E. Blomgren and P. N. Kumta, *J. Power Sources*, 2004, **130**, 275.
15 II-seok Kim and P. N. Kumta, *J. Power Sources*, 2004, **136**, 145.
16 M. K. Datta and P. N. Kumta, *J. Power Sources*, 2006, **158**, 557.
17 M. K. Datta and P. N. Kumta, *J. Power Sources*, 2007, **165**, 368.
18 H. Li, X. Huang, L. Chen, Zh. Wu and Y. Liang, *Electrochem. Solid-State Lett.*, 1999, **2**, 547.
19 M. Holpzafel, H. Buqa, L. J. Hardwick, M. Hahn, A. Wursig, W. Scheifele, P. Novak, R. Kotz, C. Veit and F.-M. Petrat, *Electrochim. Acta*, 2006, **52**, 973.
20 W. R. Liu, J. H. Wang, H. Ch. Wu, D. Ts. Shieh, M. H. Yang and N. L. Wu, *J. Electrochem. Soc.*, 2005, **152**, A1719.
21 M. Yoshio, H. Wang, K. Fukuda, T. Umeno, N. Dimov and Z. Ogumi, *J. Electrochem. Soc.*, 2002, **149**, A1598.
22 N. L. Rock and P. N. Kumta, *J. Power Sources*, 2007, **164**, 829.
23 H. Okamoto, *Phase diagrams for binary alloys*, ASM international, Materials Park, OH, 2000, p. 35.
24 J. O. Besenhard, M. Hess and P. Komenda, *Solid State Ionics*, 1990, **40–41**, 525.
25 Y. Hamon, T. Brousse, F. Jousse, P. Topart, P. Buvat and D. M. Schleich, *J. Power Sources*, 2001, **97–98**, 185.
26 M. J. Lindsay, G. X. Wang and H. K. Liu, *J. Power Sources*, 2003, **119–121**, 84.
27 H. Honda, H. Sakaguchi, Y. Fukuda and T. Esaka, *Mater. Res. Bull.*, 2003, **38**, 647.
28 M. Tillard, C. Belin, L. Spina and Y. Z. Jia, *Solid State Sci.*, 2005, **7**, 1125.
29 X. Lei, Ch. Wang, Z. Yi, Y. Liang and J. Sun, *J. Alloys Compd.*, 2007, **429**, 311.
30 P. Limthongkul, Y. Jang, N. J. Dudney and Y. M. Chiang, *Acta Mater.*, 2003, **51**, 1103.
31 M. K. Datta, S. K. Pabi and B. S. Murty, *J. Mater. Res.*, 2000, **1**, 1429.
32 C. S. Wang, G. T. Wu and W. Z. Li, *J. Power Sources*, 1998, **76**, 1.
33 W. Wang, P.N. Kumta and J. Power, *Sources*, 2007, DOI: 10.1016/j.jpowsour.2007.05.025.